α-Synuclein induced membrane remodeling is driven by binding affinity, partition depth, and inter-leaflet order asymmetry.

Anthony R. Braun†, Michael M. Lacy‡, Vanessa C. Ducas§,
Elizabeth Rhoades‡, and Jonathan N. Sachs*†

†Department of Biomedical Engineering, University of Minnesota, Minneapolis, Minnesota 55455, United States
‡Department of Molecular Biophysics and Biochemistry, Yale University, New Haven, Connecticut 06520, United States
§Department of Pediatrics, Yale School of Medicine, New Haven, Connecticut 06520, United States

Supporting Information

Protein expression, purification, and labeling

α-Syn_{100} was generated by introducing a stop codon via QuickChange mutagenesis (Stratagene) after residue 100 in a full-length α-Syn plasmid, as described previously. An α-$Syn_{NAC\text{-}null}$ construct was generated by circular polymerase extension cloning (CPEC) PCR. Primers were designed containing complementary sequences spanning residues Glu61-Gly67 and Asn79-Ala85; each primer contained an overhang with inverse complementary sequence coding for the residues EKTKEQVTNVG (lipid-binding repeat 5) to be inserted in place of the wild-type Gly68-Ala78 (lipid binding repeat 6).

A S9C mutation was introduced, also by QuickChange, to allow for site-specific fluorescent labeling. The protein was recombinantly expressed in *E. coli* and purified via ammonium sulfate precipitation followed by cation exchange at pH 4.0 and size exclusion chromatography [1]. Purity and identity of protein was verified by SDS-PAGE and mass spectrometry.

For fluorescence correlation spectroscopy (FCS) experiments, α-Syn_{100} was labeled with Alexa Fluor 488 maleimide (AL488) (Invitrogen) on the cysteine introduced at residue 9. The protein was incubated in Tris buffer (20 mM Tris, 150 mM NaCl, pH 7.4) with 10x molar excess TCEP for 5 minutes before adding 7x molar excess fluorophore for 2 hours at room temperature. Unconjugated dye was separated from the labeled protein by two stacked HiTrap desalting columns (GE Healthcare Life Sciences). UV-Vis absorbance at 495 nm was used to quantify the AL488 concentration, and the protein concentration was determined by a modified Lowry assay (Bio-Rad, Hercules, CA). Labeling efficiency (molar ratio of dye to protein) was consistently above 85%.

Vesicles

Liposomes were prepared from 100% 1-palmitoyl-2-oleoyl-sn-glycero-3-phosphoglycerol (POPG) lipid or a 1:1 mix of POPG and 1-palmitoyl-2-oleoyl-sn-glycero-3-phosphocholine (POPC) (Avanti Polar Lipids). Supplemental Figure 1A details the structure for both the zwitterionic POPC (*top*) and anionic POPG (*bottom*). Lipid powder was dissolved in chloroform to make 15-20 mg/mL stock solutions and stored at -20°C. Aliquots of this solution were dried under nitrogen stream and desiccated overnight. The resulting film was resuspended to approximately 4 mM in MOPS buffer (20mM MOPS, 147 mM NaCl, 2.7 mM KCl, pH 7.4) for at least one hour and vortexed. The resulting liposome solutions were used as is for the tubulation assays. For FCS measurements, large unilamellar vesicles (LUVs) were prepared by extruding this suspension 21 times through two stacked membranes of 50 nm pore size (Whatman) in a Liposofast extruder (Avestin). LUVs are stored at room temperature for up to several days. Before analyses, all lipid concentrations were determined by assaying for total phosphate content [2].

Fluorescence Correlation Spectroscopy

FCS measurements were made on a lab-built instrument based around an Olympus IX71 inverted microscope (Olympus, Tokyo, Japan) and a 488 nm DPSS laser (Coherent) as described previously[3]. Laser power was adjusted to 5 μW prior to entering the microscope. Fluorescence emission was collected through the objective and separated from laser excitation using a Z488rdc long-pass dichroic and an HQ600/200m band-pass filter (Chroma) and focused onto the aperture of a 50 μm optical fiber (Oz Optics, Ottawa, Canada) directly coupled to an avalanche photodiode (Pacer). A digital correlator (Flex03LQ-12, correlator.com) was used to generate the autocorrelation curve.

FCS measurements were made in 8-well chambered coverglasses (Nunc). Chambers were plasma treated and passivated by coating with polylysine-conjugated polyethylene glycol to prevent protein adsorption to the surface [4]. Binding studies were carried out at 20° C, mixing 100 nM α-Syn_{100} with various concentrations of 100% POPG or 1:1 POPG:POPC LUVs in MOPS buffer in a well (250 μL total volume) and allowing to equilibrate for 8 to 10 minutes before measuring. For each FCS measurement, 30 traces of 10 seconds each were recorded and averaged together to obtain statistical variations. The average curve was fit to an equation for multiple species of differing brightness (Equation 1) using MATLAB (The MathWorks). Further discussion of this equation can be found in [4].

$$G(\tau) = \frac{1}{N}\left(F * \frac{1}{1+\frac{\tau}{\tau_{D1}}} * \left(\frac{1}{1+\frac{s^2\tau}{\tau_{D1}}}\right)^{1/2} + Q*(1-F)\frac{1}{1+\frac{\tau}{\tau_{D2}}} * \left(\frac{1}{1+\frac{s^2\tau}{\tau_{D2}}}\right)^{1/2} \right), \qquad \text{(Eq. 1)}$$

where τ_{D1} and τ_{D2}, the diffusion times for the free protein and vesicle-bound protein, are determined by measurements of samples in the absence of lipid and with very high lipid concentration (all protein is bound), respectively and fixed to within 5% of these values for fitting curves from intermediate lipid concentrations. The structure factor *s*, the ratio of the radial to axial dimensions of the focal volume, was calibrated by measuring a solution of Alexa488 hydrazide and was fixed to 0.17. The only free parameters are: N, the number of fluorescent species; F, the fraction of protein not bound to vesicles; and Q, the average brightness of the vesicles. Binding data were fit with a hyperbolic binding curve (Equation 2) in Origin (OriginLab) to determine the K_D.

$$F' = \frac{[lipid]}{K_D + [lipid]} \qquad \text{(Eq. 2)}$$

where F' is the fraction of vesicle-bound protein, determined from fitting the FCS equation, and [*lipid*] is the molar concentration of accessible lipid, the outer membrane leaflet, calculated as 55% of the total lipid concentration.

Vesicle tubulation

To monitor remodeling of liposomes into tubular structures by α-Syn_{100}, the decrease in scattered light at 450 nm was measured as a function of time [5]. The protein was added to 100% POPG or 1:1 POPG:POPC liposomes at approximately a 1:10 protein:lipid ratio and the absorbance was monitored at 450nm with 1 nm slit width, 1 second response time in a spectrophotometer (Perkin-Elmer). 150 μL of 400 μM lipids in MOPS buffer with 1 mM TCEP was placed in a quartz cuvette and absorbance was measured every 2 seconds for at least 5 minutes to obtain a baseline signal. Appropriate amounts of α-Syn_{100} (in MOPS buffer with 1 mM TCEP) were added to achieve equivalent amounts of bound protein as determined by the quadratic binding equation (Equation 3).

$$\frac{[PL]}{[P_{tot}]} = \frac{(K_D + [P_{tot}] + [L_{tot}]) - \sqrt{(K_D + [P_{tot}] + [L_{tot}])^2 - 4[P_{tot}][L_{tot}]}}{2[P_{tot}]} \qquad \text{(Eq. 3)}$$

where $[PL]$ is the concentration of lipid-bound protein, $[P_{tot}]$ is the total concentration of protein, $[L_{tot}]$ is the total concentration of accessible lipid, and K_D is the dissociation constant calculated from the FCS measurements.

Traces were normalized to the initial lipid-only signal for each sample, and the extent of tubulation was determined by taking the average absorbance of the 50 time points from 2400-2500 sec and subtracting from the initial value. At least three replicates were performed for each lipid composition.

Simulation Methods

All simulations were run using the coarse-grained MARTINI lipid and MARTINI2.2 protein parameters[6-8]. The MARTINI forcefield applies an ~4:1 (heavy atom:CG bead) mapping, reducing the complexity of the system and allowing the study of larger systems and longer time-scales than typically accessible for all-atom resolution MD. Supplemental Figure 1B highlights the MARTINI CG representation of both POPC (*left*) and POPG (*right*) lipids (both with 13 CG-beads). Simulations were run using the GROMACS v4.5.3 program[9,10]. All systems were prepared and run in the isothermal-isobaric (NPT) ensemble with barostat and thermostat set to 1 bar and 303K respectively using a 25fs time step. Pressure coupling was performed semi-isotropically with the *xy*- and *z*-dimensions independently coupled producing an average zero surface tension. Non-bonded interactions were modeled with the standard MARTINI cut-off scheme with Lennard-Jones interactions shifted to zero between 0.9-1.2nm and electrostatic interactions in the range 0.0-1.2 nm with a uniform screening constant set at 15[6-8].

Initial equilibration included 10,000 steps steepest descent minimization followed by 2μs of dynamics using the velocity-rescaling thermostat and a Berendson barostat[9,10]. All production runs were simulated using the Nose´-Hoover thermostat and the Parrinello-Rahman barostat [11,12] with a time constant of 2.5ps and 250ps respectively. Pressure coupling was applied semi-isotropically to allow for a tensionless bilayer with uniform *x*,*y*-dimensions. All production simulations were 10μs (40μs scaled simulation time) sampled every 1ns with the last 5μs used for analysis (5000 frames).

As with all MARTINI simulations, the protein secondary structure is constrained and must be predefined[6-8]. This limitation of the MARTINI protein model precludes the direct simulation of α-Syn_{100} binding, as the binding process induces the transition from intrinsically disordered structure to an AH[13]. In this study, bound α-Syn_{100} (residues 1-100) was modeled as α-helical, except for residues 94-100 which were treated as random-coil.

Starting configurations were symmetric—having identical number of lipids (POPG and/or POPC) and proteins per monolayer—eliminating potential area-mismatch and allowing the resulting spontaneous curvature to be solely induced by the protein's perturbation to the local membrane structure. The proteins were positioned on opposite monolayer in remote regions of the periodic cell (see Supplemental Figure 1C for system construction schematic). The phase-transition temperature for both POPC and POPG is 271K, well below the 303K used for these simulations[14]. Starting configurations were constructed as follows. Two proteins were added (one per monolayer) to a pre-equilibrated 3200-lipid system (100% POPC, 1:3 POPG:POPC, 1:1 POPG:POPC, and 100% POPG) with nominal periodic dimensions ~30nm x ~30nm x ~15nm. The protein-lipid system was solvated with a minimum of 70,400 water beads and the appropriate number of counter ions to make a net neutral system.

In addition to wild-type α-Syn_{100}, three modified AH proteins (NAC-null, α-Syn:mod1, and α-Syn:mod2) were simulated to explore the effect of partition depth and binding affinity on curvature and lipid order in a consistent lipid mixture. For NAC-null, we replaced the hydrophobic NAC domain (6^{th} heptad) with a replicate of the 5^{th} heptad (GAVVTGVTAVA ➔ EKTKEQVTNVG). For α-Syn:mod1 the following mutations were made to make the protein more hydrophobic: K10L, K12L, E13L, K23L, K34L, E35L, K43L, E57L, K58L, and K96L. α-Syn:mod2 mutations were made to make the protein more hydrophilic: V16K, A17E, A27K, L30K, V70T, V71E, T75E, S87E, and I88K. NAC-null was simulated in pure POPG. α-Syn:mod1 was simulated in 100% POPC and α-Syn:mod2 was simulated in 100% POPG as well as 100% POPC. All α-Syn mutation systems were simulated following the same protocol detailed above.

The 400:1 systems were built with the same random configuration of 8-αS on one monolayer. Lipids were inserted into both top and bottom monolayers with 23-lipids pre protein removed from the protein leaflet to insure no excess area drives the curvature induction[1]. The system was solvated with 70,400 water beads and the appropriate number of counter ions.

The tubule simulations were built with a local protein:lipid ratio of 1-50 (within the region of membrane containing the protein). Three unique protein conformations were studied, each with 48 α-Syn_{100} protein: 1) the Spoke conformation has radially aligned α-Syn_{100} proteins with a 7.5° angle between neighboring proteins; 2) the Circumferential conformation has 7-circumfrential rings of α-Syn_{100}, initially separated by two lipid shells; and 3) the Carpet conformation is a linear array of 8 rows of 6 α-Syn_{100}, also initially separated with two shells of lipids. Each protein structure spanned a membrane region with a mean diameter of ~40nm. The total periodic cell for each system was approximately 170nm x 170nm x 30nm. For each conformation, 48 proteins were placed on an asymmetric bilayer comprised of 85,296 POPG lipids, where 23-lipids per protein were removed from the top monolayer (1,104 in total),

3,996,000 CG waters (10% antifreeze, a solvent beads used in the MARTINI forcefield that ensures local heating/cooling effects do not nucleate freezing of the CG water) and counter ions for a total of 5,200,608 CG beads. Removing excess lipids to minimize potential area mismatch insures that curvature induction is solely driven by local bilayer remodeling. This is a key difference between our approach and that used to simulation tubulation by BAR domain proteins[15,16].

In the tubulation experiment, the entirety of the vesicle surface would be adorned with α-Syn_{100}, and the formation of the nucleation structure would result from spontaneous alignment of a α-Syn_{100}. The goal of this simulation was to explore how curvature reinforcement due to aligned α-Syn_{100} helices can propagate macroscopic remodeling.

All of the tubule simulations were run for at least 300ns (the spoke conformation out to 850ns). Our previous work has show a preference for α-Syn_{100} to associate with membrane regions that have positive curvature (e.g. a hill)[1]. Indeed, if these simulations were extend into 10s to 100s of microseconds, the proteins may diffuse apart and the organized protein structure may become disordered. However we speculate that the curvature sensing properties of α-Syn would drive further alignment of other bound proteins dispersed on the flat region of the membrane (not present in these simulations) and not lead to the loss of the pre-aligned nucleating structure. This process would further facilitate the extrusion of the tubule. Indeed, in the carpet conformation we the rectangular grid is becoming pinched off as the proteins begin to align in a more radial arrangement. See Supplemental Figure 9D.

Data Analysis

Trajectories were manipulated and processed using both the GROMACS v.4.5.3 simulation package[9,10] and the MDAnalysis python library[17]. Further data analysis and figure rendering was performed using MATLAB (v.R2012a).

Surface Rendering and Curvature Determination

Curvature analysis to determine $\langle h(x,y)\rangle$ was performed without modification as detailed in [1]. Briefly, PO_4 beads for every lipid were used to define each monolayer. The undulation reference surface (URS) which defines the local mid-plane of the bilayer is rendered using the direct Fourier method with a filter cutoff of q_0 = 1.5 nm^{-1}. All surfaces were oriented to center each protein at the origin, aligning the protein's longitudinal axis with the *x*-axis. Individual protein $h(x,y)$ were averaged per frame, then subsequent averaged across the production simulation. Analysis of the undulation spectrum indicated convergence of undulation amplitudes with a 5 μs window for simulation times greater than 5 μs.

Surface area for $\langle h(x,y)\rangle$, $A_{h(x,y)}$, was determined using a summation over Fourier coefficients for the surface as described in [18]. The percent increase in surface area is determined as $1 - A_{h(x,y)}/A_{xy}$, where $A_{h(x,y)}$ is the true area, A_{xy} is projected area.

Number Density Profiles

Number density profiles were determined using the undulation correction method detailed in [18]. Briefly, the URS for each frame was defined using the lipid PO_4 bead and applying a low-pass spatial filter (cutoff = 1.5 nm^{-1}) on the corresponding Fourier coefficients. The local position for every bead on the URS was used to correct for the long-wavelength fluctuations the broaden the bilayers structure. Beads corresponding to each lipid component, solvent, and protein were binned and their corresponding component densities used to describe the membrane structure. The hydrophobic thickness (D_C) of the membrane was defined as the *z*-position where it was both solvent or acyl-chain bead were equally probable.

Total Lipid Order Parameters, $S_z(\bar{x},\bar{y})$

The local total lipid order parameter, $S_z(\bar{x},\bar{y})$, was averaged over all tail segments and parsed by leaflet and binned relative to spatial orientation about the protein as

$$S_z(\bar{x},\bar{y}) = \frac{1}{n_b}\sum_{i=1}^{n_b}\frac{1}{2}(3\langle\cos^2\theta_i(x,y)\rangle - 1)\,, \qquad \text{(Eq. 4)}$$

where $\bar{x},\bar{y}$ denote a uniform grid of points centered about the protein aligned to the *x*-axis, n_b is the number of acyl-chain bonds per lipid and $\theta_i(x,y)$ is the angle between the i^{th} bond vector and the local bilayer normal (determined from the URS) at a particular *xy*-position about the protein. The resulting $S_z(\bar{x},\bar{y})$ field allows us to observe local perturbations to the order due to protein insertion where values of 1, 0, and -0.5 correspond to perfect alignment,

random orientation, and anti-alignment with the local bilayer normal respectively. $S_z(\bar{x},\bar{y})$ was determined by averaging over the last 5 μs of the production run, sampling every nanosecond.

The tubule $S_z(\bar{x},\bar{y})$ was oriented relative to the center of the protein structure with the same protein aligned with the *x*-axis for each frame. Due to rapid deformation of the membrane, a shorter window (20 ns) was used to capture effects at the beginning (0 to 20 ns) and end (830 to 850 ns) of the formation of the budding tubule.

Inter-leaflet acyl-chain contacts

The development of symmetric, anti-aligned order parameters across the bilayer suggest that the acyl-chains may experience increased chain-chain contacts, stabilizing the anti-aligned conformation. The number of acyl-chain contacts was determined for lipids both near the protein and in bulk, by calculating the total number of acyl-chain beads in the opposite leaflet at a given distance. The first peak corresponds to first shell contacts and provides a measure of total acyl-chain-to-acyl-chain inter-leaflet contacts in a specific region of the membrane.

Distance Matrix and Protein-Protein Angle Analysis

Distance matrices for the 400:1 systems were determined for all protein-protein interaction pairs by calculation of all residue-residue distances (two unique interactions per pair, see Supplemental Figure 5A). The two distances were parsed based on minimum and maximum into two separate distance matrices. The mean distance across all interactions was used to define the global distance between any two proteins. This global distance was used to subsequently bin protein-interactions of similar length to extract the relevant neighbor protein interaction motifs. Nearest neighbor protein interactions all contained an average distance < 15nm with a majority of protein-protein interactions falling within < 9nm average distance.

To determine the range of conformational space sampled by each system a 10ns averaging window was applied across the 10μs production run, yielding 1000 different minimum residue-residue interactions per system. Due to time-scale limitations implicit to CGMD simulations, we have not fully sampled all of configurational space. Each 400:1 system was constructed and started from identical starting configurations, thereby introducing the same starting configuration bias across systems. The minimum protein-protein distance sampled a range of different residue-residue interaction pairs (see Supplemental Figure 5A). We characterized the range of sampling by the percent of unique residue-residue minimum distances sampled relative to the total number of possible residue-residue interactions. A unique residue-residue interaction was one that was not previously sampled earlier in the trajectory.

Modified α-Syn$_{100}$*: Explores partition depth effects on spontaneous curvature*

For completeness, we have also simulated α-Syn$_{100}$ in 1:3 PG:PC and pure POPC. Although no experimental data is available for comparison, as binding affinities are very low in these systems, they are at the least useful for discussion purposes and show very similar results as 1:1 PG:PC (Supplemental Figure 2A).

We engineered two modified α-Syn$_{100}$ proteins (α-Syn:mod1 and α-Syn:mod2) through numerous point mutations that allow us to explore the curvature/lipid order correlation within a specific lipid composition. α-Syn:mod1 was engineered to be more hydrophobic, disrupting salt-bridges between positive LYS residues and the negative PO_4 bead. In contrast, α-Syn:mod2 was engineered to be more hydrophilic, mutating a series of VAL and ALA into LYS and GLU (full detail of specific mutations presented in Supporting Information).

Number density profiles for both α-Syn:mod1 and α-Syn:mod2 in 100% POPC and 100% POPG are presented in Supplemental Figure 6 (panels A. and B. respectively). The more hydrophobic α-Syn:mod1 partitions deeper in the POPC membrane relative to α-Syn$_{100}$, resulting in a reduction in spontaneous curvature. In contrast, the hydrophilic α-Syn:mod2 partitions further out from the acyl-chain core in POPC (in POPG, both proteins partitioned to a similarly more shallow depth, only α-Syn:mod2 is presented, Supplemental Figure 4B). As predicted, when the protein partitions less deep into the acyl-chain core there is a concomitant increase in both curvature and lipid order asymmetry (Supplemental Figure 6C), providing direct *in silico* evidence supporting May's AH curvature theory[19].

References

(1) Braun, A. R.; Sevcsik, E.; Chin, P.; Rhoades, E.; Tristram-Nagle, S.; Sachs, J. N. *J Am Chem Soc* **2012**, *134*, 2613.

(2) Chen, P. S.; Toribara, T. Y.; Warner, H. *Anal. Chem.* **1956**, *28*, 1756.

(3) Trexler, A. J.; Rhoades, E. *Biochemistry* **2009**, *48*, 2304.

(4) Middleton, E. R.; Rhoades, E. *Biophys J* **2010**, *99*, 2279.

(5) Varkey, J.; Isas, J. M.; Mizuno, N.; Jensen, M. B.; Bhatia, V. K.; Jao, C. C.; Petrlova, J.; Voss, J. C.; Stamou, D. G.; Steven, A. C.; Langen, R. *J. Biol. Chem.* **2010**, *285*, 32486.

(6) Monticelli, L.; Kandasamv, S. K.; Periole, X.; Larson, R. G.; Tieleman, D. P.; Marrink, S. J. *Journal of Chemical Theory and Computation* **2008**, *4*.

(7) Marrink, S. J.; Risselada, H. J.; Yefimov, S.; Tieleman, D. P.; de Vries, A. H. *Journal of Physical Chemistry B* **2007**, *111*, 7812.

(8) de Jong, D. H.; Singh, G.; Bennett, W. F. D.; Arnarez, C.; Wassenaar, T. A.; Schäfer, L. V.; Periole, X.; Tieleman, D. P.; Marrink, S. J. *Journal of Chemical Theory and Computation* **2013**, *9*, 687.

(9) Van der Spoel, D.; Lindahl, E.; Hess, B.; Groenhof, G.; Mark, A. E.; Berendsen, H. J. C. *Journal of Computational Chemistry* **2005**, *26*, 1701.

(10) Hess, B.; Kutzner, C.; van der Spoel, D.; Lindahl, E. *Journal of Chemical Theory and Computation* **2008**, *4*, 435.

(11) Parrinello, M.; Rahman, A. *J. Appl. Phys.* **1981**, *52*, 7182.

(12) Nose ´ , S.; Klein, M. L. *Mol. Phys.* **1983**, *50*, 1055.

(13) Maltsev, A. S.; Chen, J.; Levine, R. L.; Bax, A. *J Am Chem Soc* **2013**, *135*, 2943.

(14) Pan, J. J.; Heberle, F. A.; Tristram-Nagle, S.; Szymanski, M.; Koepfinger, M.; Katsaras, J.; Kucerka, N. *Bba-Biomembranes* **2012**, *1818*, 2135.

(15) Arkhipov, A.; Yin, Y.; Schulten, K. *Biophys J* **2009**, *97*, 2727.

(16) Yin, Y.; Arkhipov, A.; Schulten, K. *Structure* **2009**, *17*, 882.

(17) Michaud-Agrawal, N.; Denning, E. J.; Woolf, T. B.; Beckstein, O. *Journal of Computational Chemistry* **2011**.

(18) Braun, A. R.; Brandt, E. G.; Edholm, O.; Nagle, J. F.; Sachs, J. N. *Biophys J* **2011**, *100*, 2112.

(19) Zemel, A.; Ben-Shaul, A.; May, S. *Journal of Physical Chemistry B* **2008**, *112*, 6988.

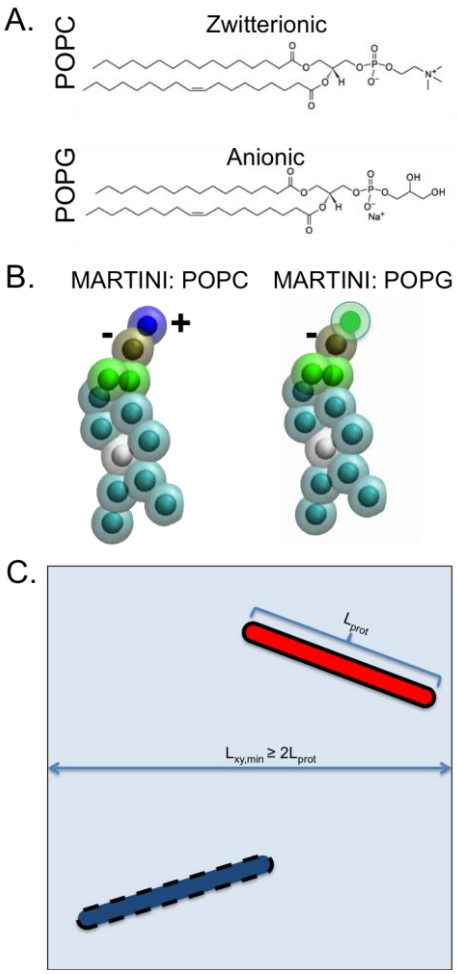

Supplemental Figure 1. A. Chemical structure of zwitterionic POPC (*top*) and anionic POPG (*bottom*). Both lipids have identical acyl-chains and phase transition temperature. B. MARTINI representation of a single POPC lipid (*left*) and POPG (*right*) with non-polar beads (*cyan*, *white*), polar beads (*green*), negatively charged PO_4 bead (*brown*) and positively charged choline (*blue*) (13 CG-beads). The MARTINI lipid forcefield applies a 4:1, heavy-atom to CG-bead mapping, significantly reducing the computational cost to run large length scale and long time scale simulations. C. Schematic for the construction of the symmetric 2-protein systems. Periodic box dimensions are defined to ensure a minimal distance of 2-protein lengths.

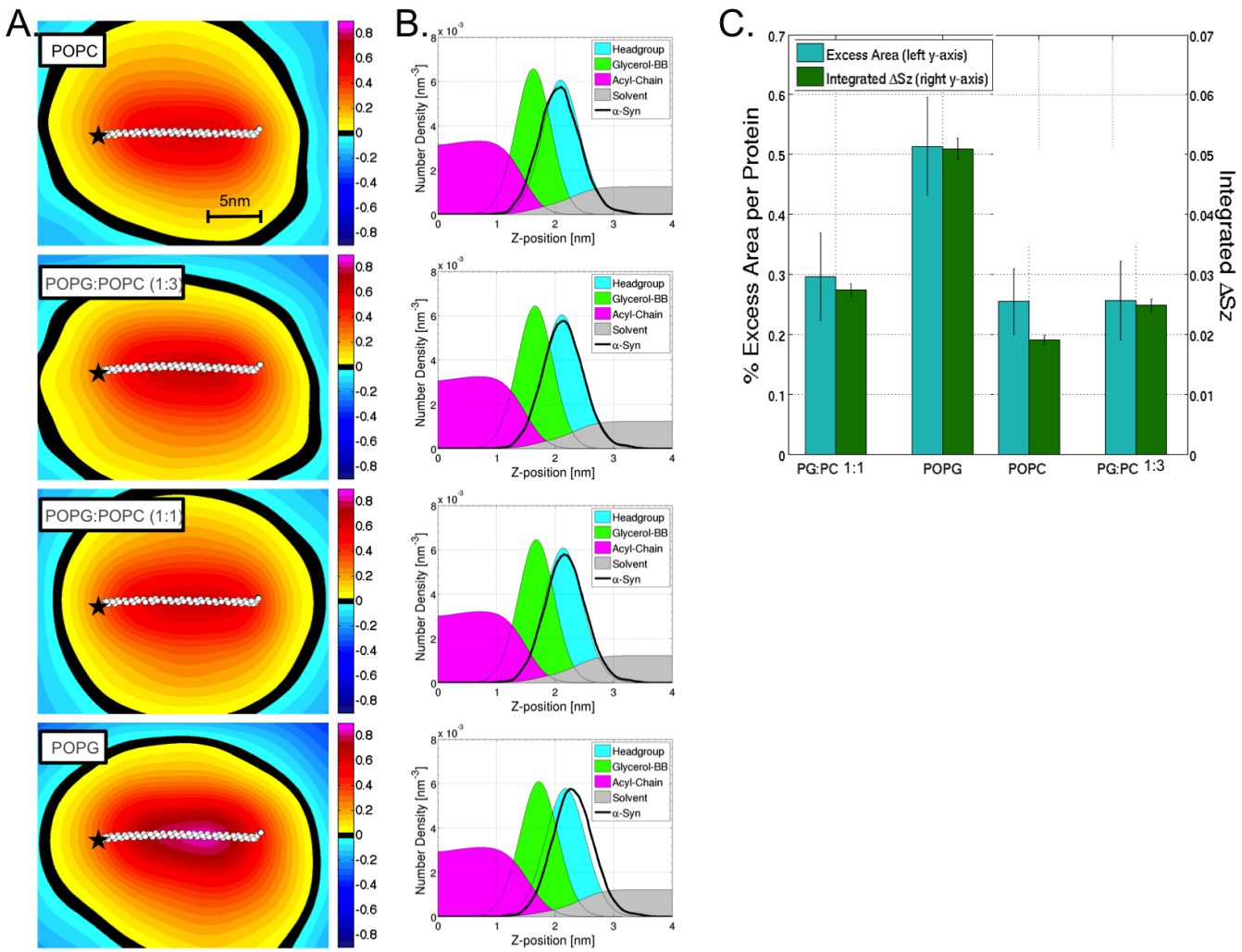

Supplemental Figure 2. A) Time-averaged height surfaces, $\langle h(x,y)\rangle$, for four α-Syn$_{100}$ systems (POPC-*top*, PG:PC 1:3-*middletop*, PG:PC 1:1-*middlebottom*, POPG-*bottom*). Color-map units are nm. B) Number density profiles for α-Syn$_{100}$ (*black*-line) for all systems illustrate decreased partition depth for POPG relative to POPC or both PG:PC systems. N-terminus of α-Syn$_{100}$ indicated with . C. Comparison of percent excess area per protein and total lipid-order asymmetry for the four α-Syn$_{100}$ systems.

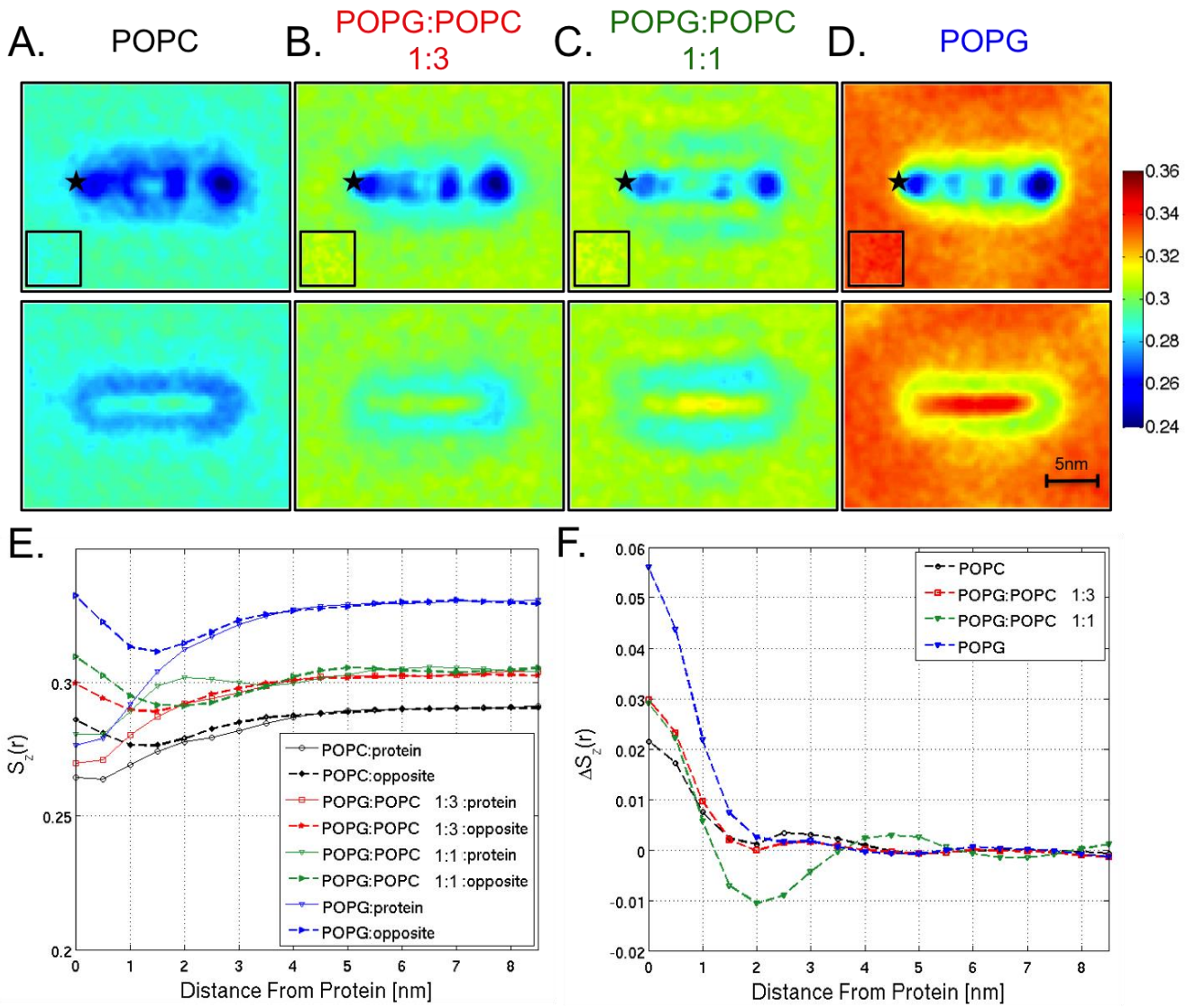

Supplemental Figure 3. A-C) Local total order parameter $S_z(\bar{x},\bar{y})$ for POPC, POPG:POPC 1:3, and POPG respectively for the protein leaflet (*top*) and opposing leaflet (*bottom*), warm colors are more ordered, cool colors more disordered. Inset panels in A-C *top* correspond to the pure lipid $S_z(\bar{x},\bar{y})$ for each mixture respectively. Colormap is a global scale used for each panel. D) Average $S_z(r)$ for both leaflets of each system (POPC *black*, POPG:POPC *red*, POPG *blue*; opposite leaflet in bold). E) The ΔS_z, *opposite leaflet – protein leaflet*, illustrates in increasing difference across the bilayer for increased charge density (POPC < POPG:POPC < POPG). N-terminus of α-Syn_{100} indicated with .

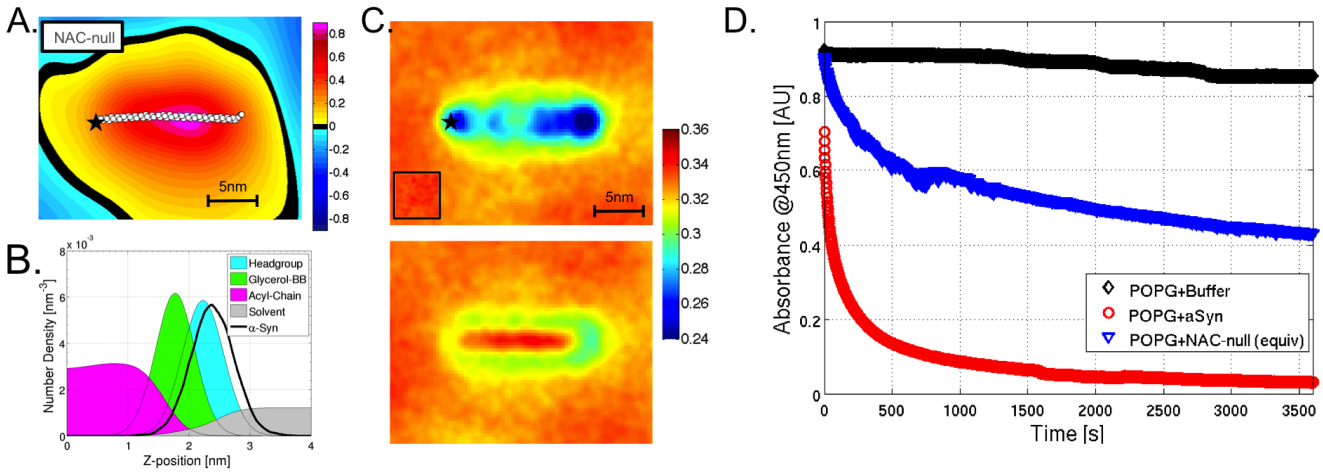

Supplemental Figure 4. Analysis of NAC-null system. A. Time-averaged height surfaces, $\langle h(x,y)\rangle$. Color-map units are nm. B) Number density profile shows similar partitioning as WT:α-Syn$_{100}$ in POPG. C. Two-dimensional total lipid order maps for the protein monolayer (*top*) and opposite monolayer (*bottom*) with pure POPG illustrated in the *inset*. D. Vesicle clearance assay absorbance time course for NAC-null compared to WT:α-Syn$_{100}$ in POPG show intermediate tubulation capacity. In panels A. and C., the protein's N-terminus indicated with .

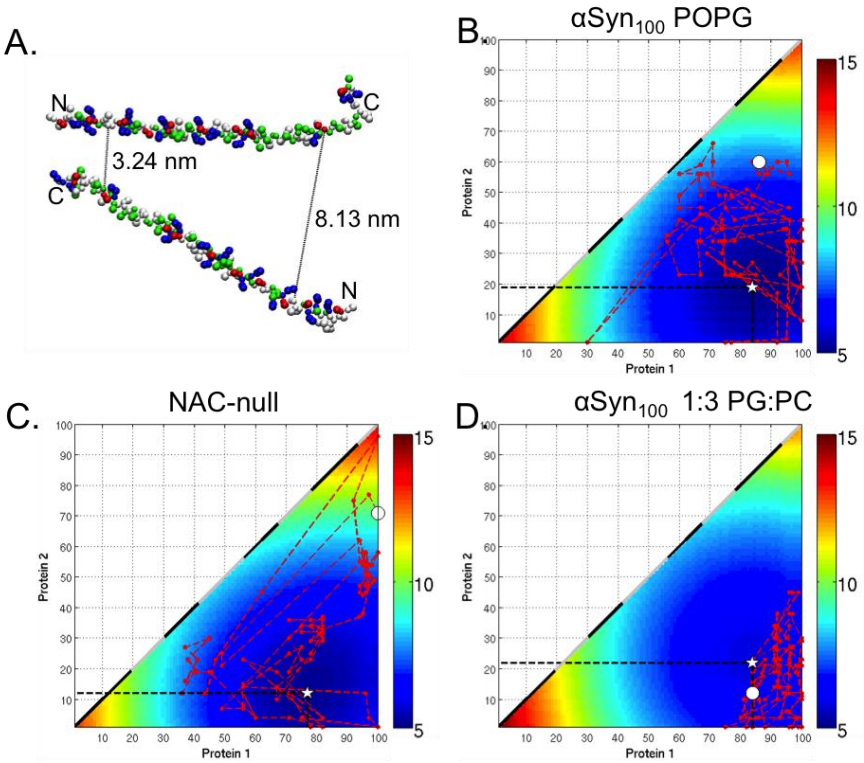

Supplemental Figure 5. A) Snapshot of an anti-parallel α-Syn_{100} protein interaction pair highlighting residue-residue distances (17 to 83). Each protein interaction pair contains two residue-residue distances. These distances are parsed into minimum and maximum distance matrices. B-D) Minimum distance matrices for α-Syn_{100} (B), NAC-null (C), and α-Syn_{100} in 1:3 PS:PC (D) averaged across the last 5μs. *Red* '--*' indicating sequential minimums from a 10ns windows. The starting minimum distance residue-residue interaction is indicated by the white 'O', and the minimum distance for the 5μs average by '☆'.

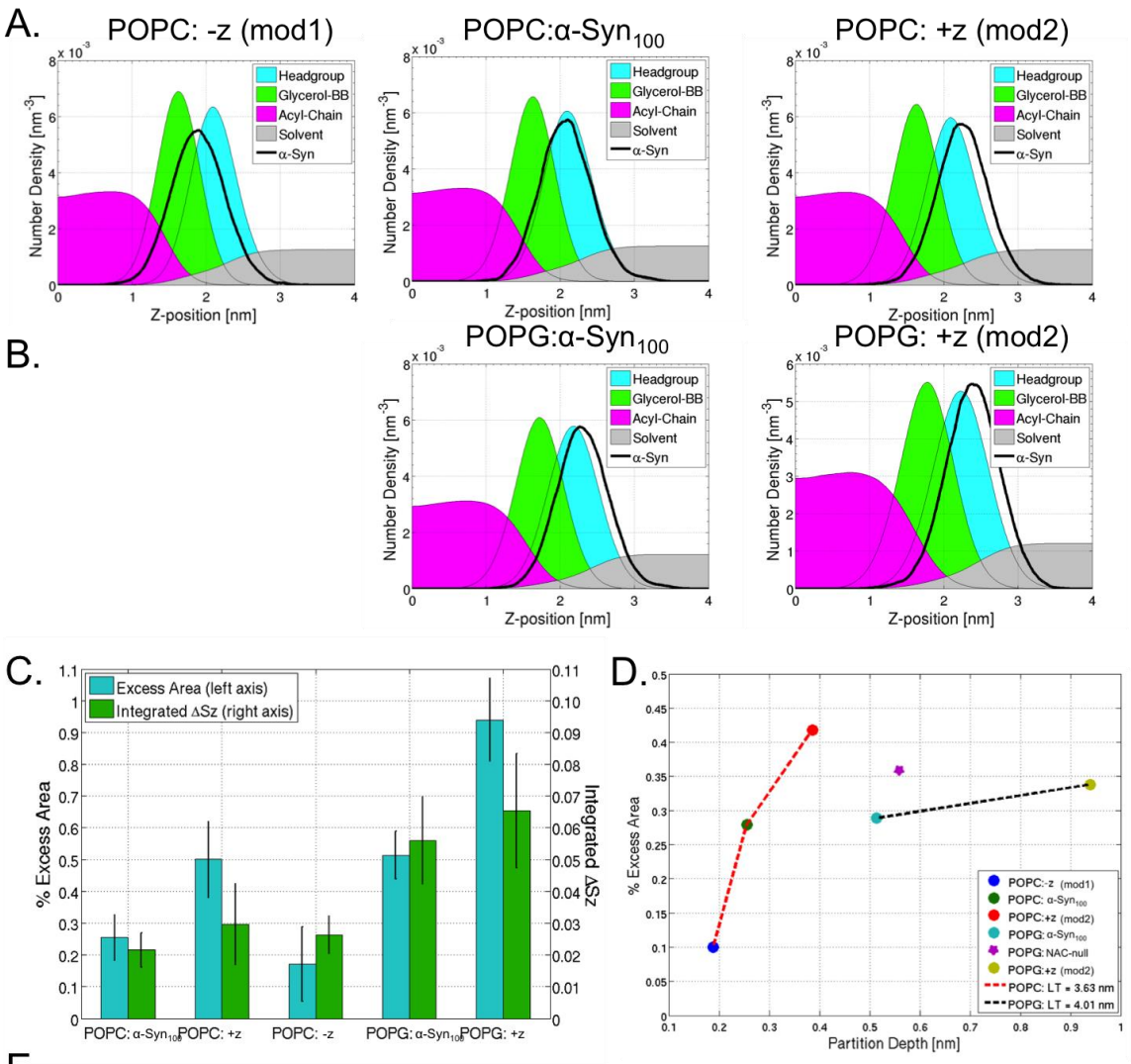

E.

	% Excess Area	D_C [nm]	Z_{pep} [nm]	Z_{pep}-D_C [nm]
POPC+αSyn:mod1	0.19	1.81	1.91	0.10
POPC+αSyn$_{100}$	0.25	1.82	2.10	0.28
POPC+αSyn:mod2	0.38	1.83	2.24	0.42
POPG+αSyn$_{100}$	0.51	1.97	2.25	0.29
POPG+αSyn:mod2	0.93	2.04	2.38	0.34

Supplemental Figure 6. A. Number density profiles for the modified and WT α-Syn$_{100}$ in 100% POPC. Each row corresponds to a different protein construct: *top*, α-Syn:mod1; *middle*, α-Syn:WT; *bottom*, α-Syn:mod2. Number density profiles detail lipid headgroup (*cyan*), glycerol-carbonyl (*green*), acyl-chain (*purple*), solvent (*gray*) and protein (*black*-line). B. Number density profiles for α-Syn$_{100}$ and α-Syn:mod2 in 100% POPG. C. Comparison of excess area per lipid (*cyan*) and integrated lipid order asymmetry (*green*) for α-Syn:mod1,2 systems relative to α-Syn:WT. D. Trends in partition depth versus percent excess area for five systems: POPC:mod1 (•); POPC: α-Syn$_{100}$ (•); POPC:mod1 (•); POPG: α-Syn$_{100}$ (•); and POPG:mod1 (•). POPC systems have a hydrophobic thickness $2D_C$ of 3.63nm (*red* dashed-line), and POPG systems have a hydrophobic thickness of 4.01nm (*black* dashed-line). Partition depth corresponds to distance from the point of equal-probability of finding solvent or acyl-chain beads. E. Summary of curvature and protein partition results for α-Syn:WT and mod1,2 proteins in POPC (*green*) and POPG (*purple*).

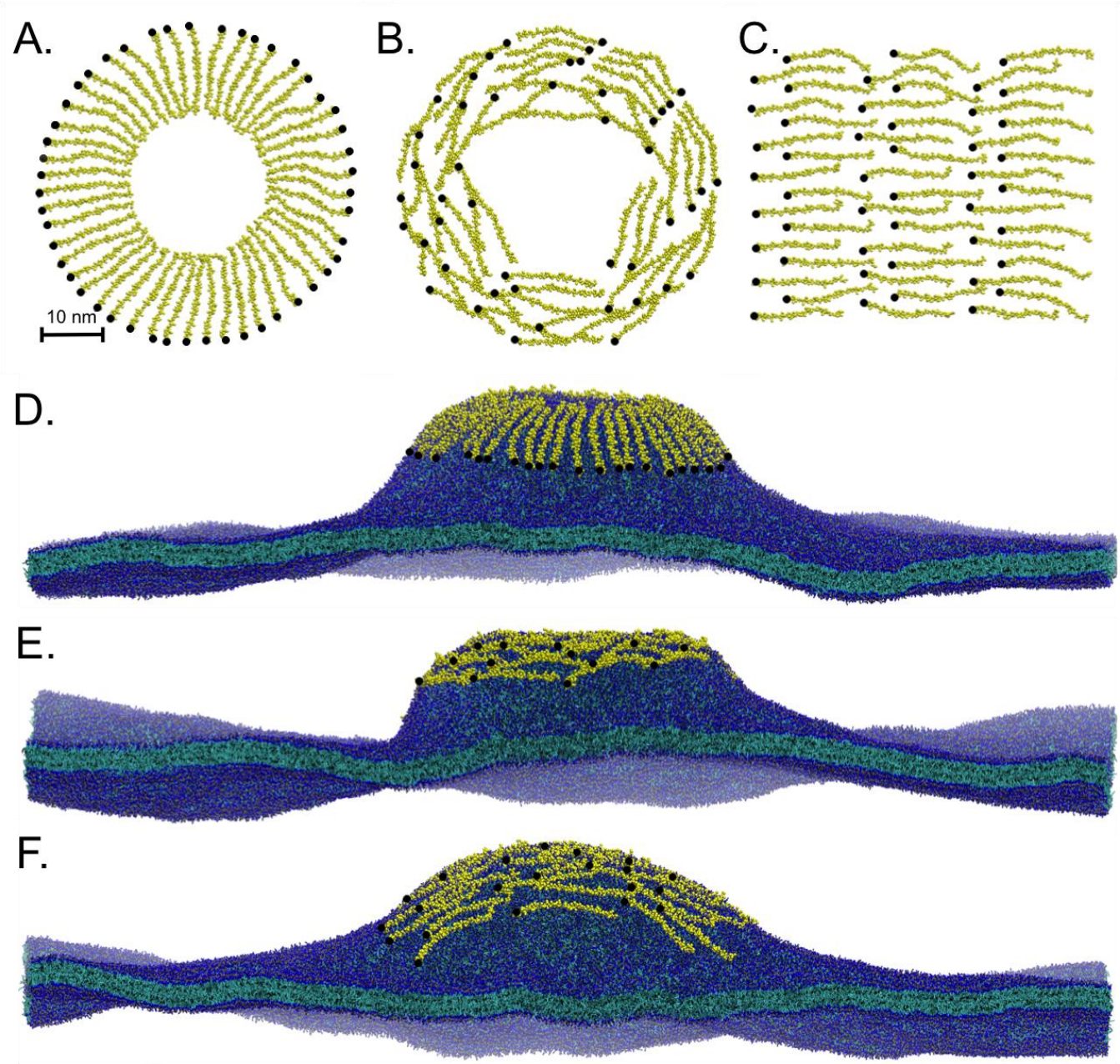

Supplemental Figure 7. Protein starting conformations for A. Spoke; B. Circumferential; and C. Carpet protein configurations. Each system started from a flat membrane at t=0ns. Snapshot at 300ns for D. Spoke; E. Circumferential; and F. Carpet systems. N-terminus of each protein indicated by •.

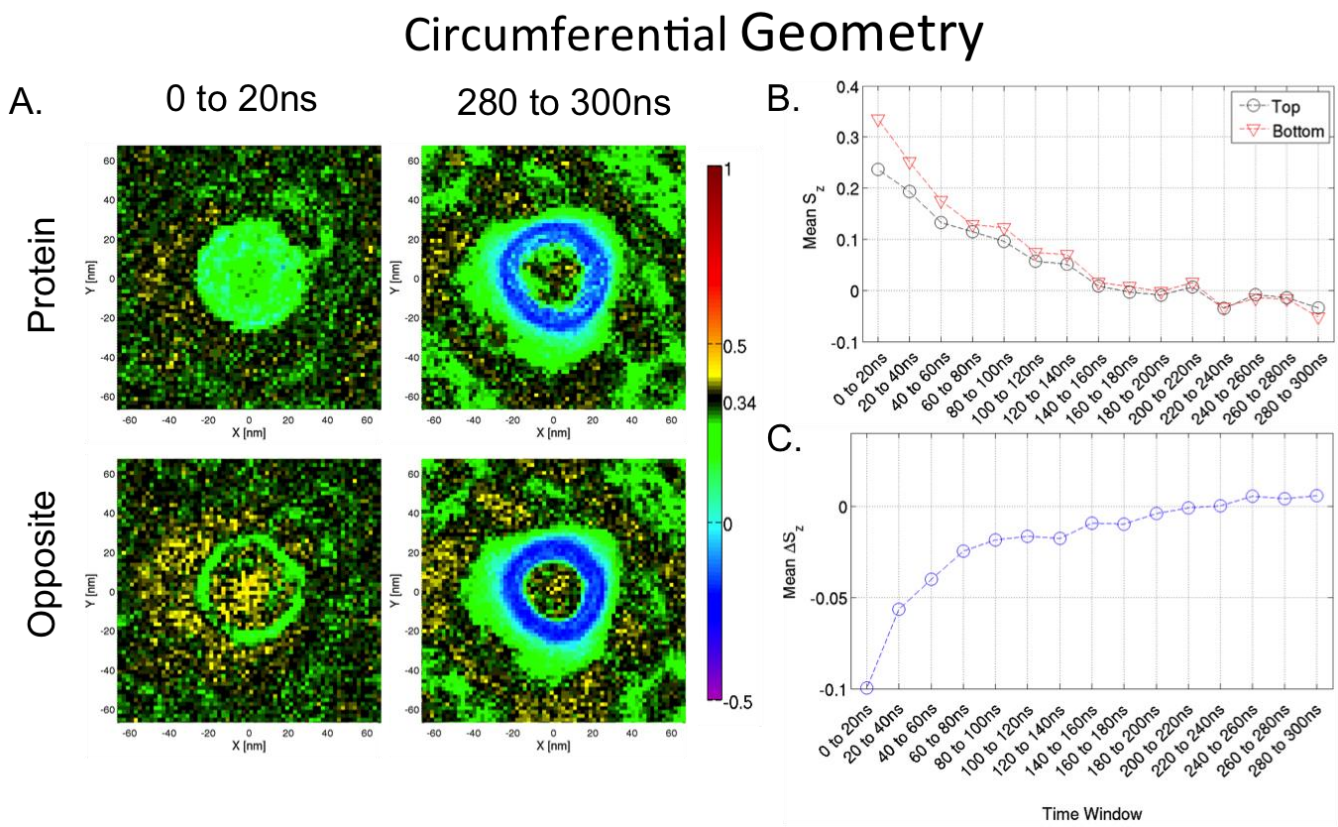

Supplemental Figure 8. A) $S_z(\bar{x},\bar{y})$ for protein (*top*) and opposite (*bottom*) monolayers at early stage (0 to 20ns, *left*) and late tubule stage (280 to 300ns, *right*) for the circumferential protein conformation. Color map reference (*black*) set at S_z for pure POPG. B) Time course for mean S_z for the protein (*black*) and opposite (*red*) monolayers as tubule develops. C) Average difference, ΔS_z, across the membrane ($S_{z,opposite}$ - $S_{z,protein}$).

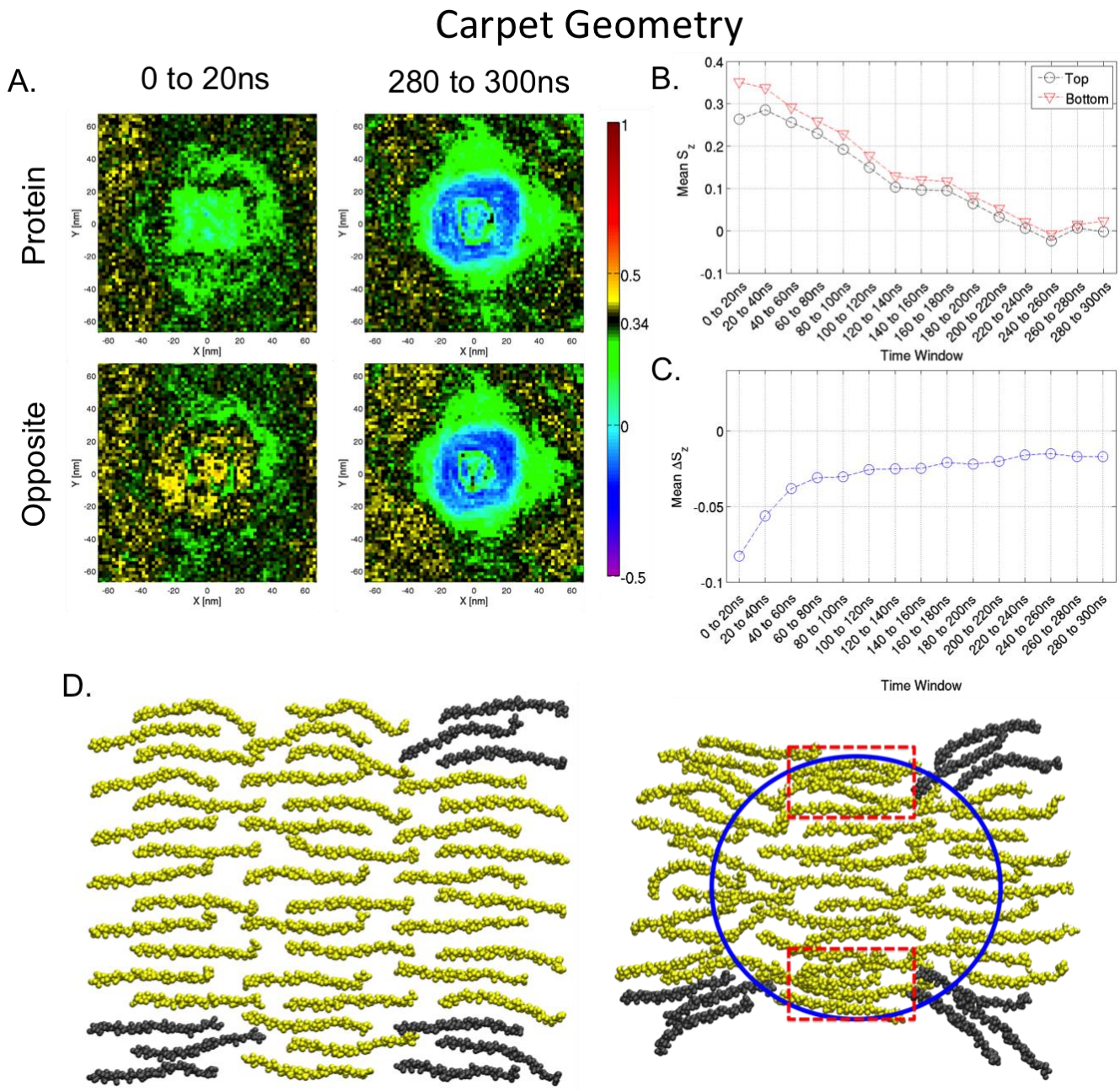

Supplemental Figure 9. A) $S_z(\bar{x}, \bar{y})$ for protein (*top*) and opposite (*bottom*) monolayers at early stage (0 to 20ns, *left*) and late tubule stage (280 to 300ns, *right*) for the carpet protein conformation. Color map reference (*black*) set at S_z for pure POPG. B) Time course for mean S_z for the protein (*black*) and opposite (*red*) monolayers as tubule develops. C) Average difference, ΔS_z, across the membrane ($S_{z,opposite}$ - $S_{z,protein}$). D. Protein conformations for 0ns (*left*) and 300ns (*right*) showing the how regions in the carpet conformation are beginning to radially align (*gray protein*) while others are forming a tight packed circumferential (*red* dashed box).

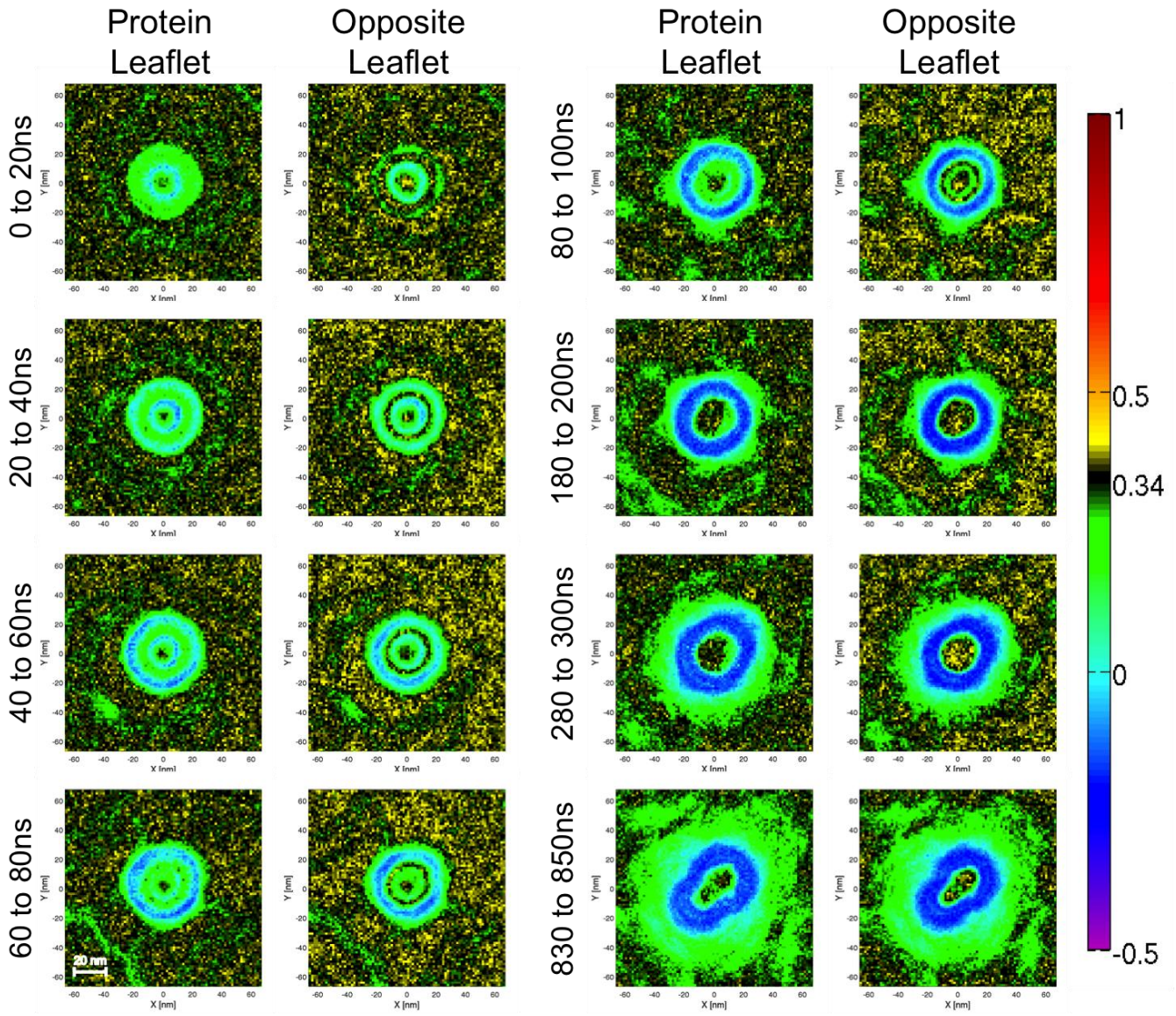

Supplemental Figure 10. Nucleation of a tubule with the spoke conformation demonstrates a drive toward symmetric total order parameters, $S_z(\bar{x},\bar{y})$. Bracketed in 20ns windows, each set of panels illustrates the order parameters for the protein leaflet (*left*) and opposite leaflet (*right*). Color-map is defined such that S_z for pure POPG is *black*, decreased order is *green*, random is *light blue*, and anti-alignment are darker blue. All $S_z(\bar{x},\bar{y})$ were determined relative to the local bilayer normal.

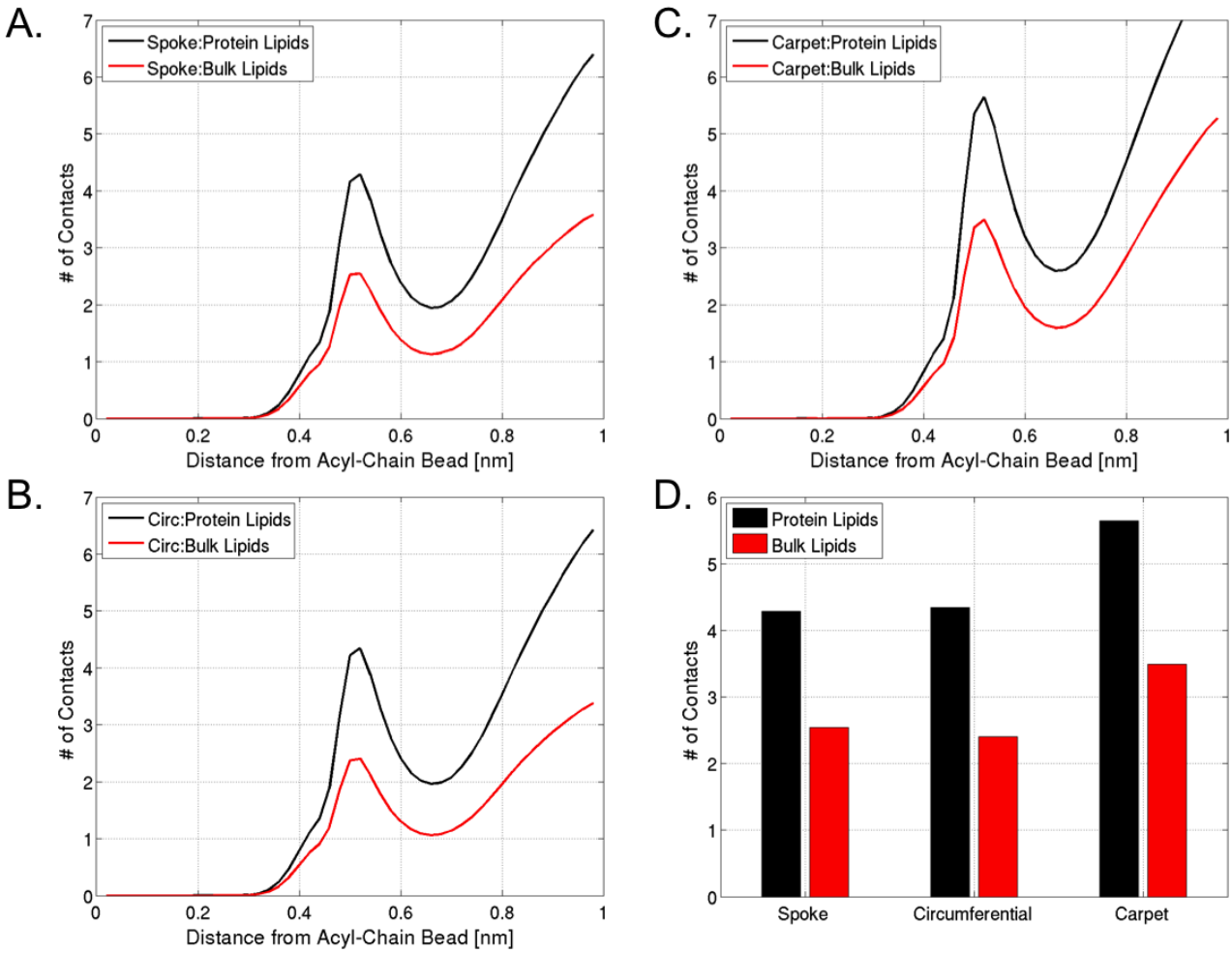

Supplemental Figure 11. Quantification of inter-leaflet acyl-chain contacts. A., B., and C. Acyl-chain-to-acyl-chain contacts across the bilayer for the spoke, circumferential, and carpet systems respectively. D. Isolation of the first-shell contacts for each system highlights a nearly 2-fold increase in inter-leaflet contacts.

Supplemental Table 1. CGMD results for protein depth, hydrophobic thickness, and curvature capacity.

	% Excess Area	D_C [nm]	Z_{pep} [nm]	Z_{pep}-D_C [nm]
POPC +αSyn_{100}	0.25	1.82	2.1	0.28
PG:PC 1:3 +αSyn_{100}	0.26	1.86	2.15	0.29
PG:PC 1:1 +αSyn_{100}	0.3	1.89	2.15	0.26
POPG +αSyn_{100}	0.51	1.97	2.25	0.28
POPG +NACnull	0.56	2.01	2.37	0.36
400:1 POPG +αSyn_{100}	0.48	2.02	2.09	0.07
400:1 POPG +NACnull	0.3	2.02	2.15	0.13
400:1 PG:PC 1:3 +αSyn_{100}	0.24	1.89	1.97	0.08
POPC (pure lipid)	-	1.81	-	-
PG:PC 1:3 (pure lipid)	-	1.84	-	-
PG:PC 1:1 (pure lipid)	-	1.87	-	-
POPG (pure lipid)	-	1.94	-	-